Collision rate constant for non-spherical particles moving under shear flow

Frédéric Gruy, Patrice Nortier

Collision Rate Constant for Non-Spherical Particles Moving under Shear Flow

Frédéric Gruy, Patrice Nortier

Ecole Nationale Supérieure des Mines, 158 cours Fauriel, 42023, Saint-Etienne, Cedex 02

Corresponding author: Frédéric Gruy, fgruy@emse.fr

Abstract: Taking into account the morphology of the particles in the aggregation dynamics is addressed theoretically in this paper. The rate constant or kernel of collision between particles with simple shapes (spheroids oblate and prolate, disc, needle) has been calculated from a Monte Carlo algorithm simulating shear aggregation. The corresponding data were used to build a model, which comes in the form of an empirical expression linking the rate constant of collision, the shear rate and three shape parameters describing each particle. This concise expression represents very well all the data issued from Monte Carlo calculation. Statistical analysis of the Monte Carlo calculations and the proposed model as well has been carefully achieved.

keywords : shear aggregation, convex particles, anisotropic particles, Monte Carlo Simulation, analytical modelling

Introduction

Aggregation of fine particles is a phenomenon frequently met during the synthesis of particles by precipitation or crystallization, in suspensions containing a precursor of ceramics, in aerosols...Aggregation of particles in a fluid depends on several phenomena. The collision between two primary particles can arise from the Brownian motion, the fluid and particle velocity fields. So, Von Smoluchowski has calculated the collision rate for spheres in the case of Brownian motion and particles moving in a shear flow [1,2]. This approach has been extended to spherical particles moving in a turbulent flow [3] or a rarefied atmosphere [4]. As

a consequence, a collision rate constant has been calculated for each mechanism. In its early history, aggregation has been strongly related to colloids science where physico-chemical aspects are prevailing. So, Van der Waals and Electric Double Layer interactions have been identified and constitute the basis of DLVO theory [5, 6]. This one addresses the stability of the particle suspension. Fuchs [7] established the link between aggregation rate constant and inter-particle interaction by introducing a multiplicative factor into the expression of the collision rate constant. By a similar way, Spielman [8] and Zeichner et al. [9] introduced the effect of the hydrodynamic resistance on aggregation rate. Later refinements have included retarded Van der Waals interaction, non DLVO forces, roughness parameters, non-wetting effect [10]. Therefore, aggregation kernel is now written as the product of the collision rate constant and the aggregation efficiency. At the scale of the colliding primary particles, the impact of the particle asphericity has not been rigorously treated. The considered geometrical parameter is only the radius of the volume equivalent sphere. Brownian aggregation is the predominant mechanism for nanoparticles in aqueous suspension whereas shear aggregation is the one for micro-particles. The two mechanisms occur at the same time for particles sized within the [0.1-1µm] range [11]. The experimental validation of the mentioned models and theories is based on the study of the first instants of aggregation, for whom only doublets of primary particles are formed [12].

At the later instants of aggregation, clusters of primary particles are formed. Simulations, e.g. Monte-Carlo simulations, make it possible their computational formation [13-16]. Statistical analysis of the clusters formed by basic mechanisms shows that the larger ones have a fractal-like structure, i.e. porous objects with self-similar spatial ordering. Collision between aggregates has to take account of their permeability as well [17, 18]. However, the comparison between these simulations and experiments suggests that internal mechanisms as restructuring, sintering between primary particles and fragmentation occur [19-26]. The resulting aggregates are more compact and elongated. Consideration of such phenomena in simulations is yet under study.

Moreover the dynamics of the population of interacting and merging aggregates may be modeled by solving a population balance equation. Aggregates are roughly depicted by one internal variable (the volume of matter or the radius of the volume equivalent sphere or the radius of the spherical hull) and, possibly, another one (porosity or fractal dimension). In the special case of homogeneous kernel the population density reaches a self-preserving shape [27-29]. In the other cases the complexity and the large variety of phenomena affecting the

aggregation kinetics and the morphology changes restrict complete and realistic description of the aggregate population to date.

On the other hand, the synthesis of particles with controlled morphology has developed since the pioneering work of Matijevic [30, 31]. The authors strove to control the shape and size of the particles and to understand the mechanisms of synthesis. However, few studies have been dedicated to the aggregation of non-spherical primary particles. Unfortunately they do not correspond to shear aggregation [32] or consider only the late stage of aggregation in relation with the suspension rheology [33]. Quantitative studies about kinetics often consider the amount of matter and therefore the radius of the volume equivalent sphere as the relevant parameter involved in the modelling of the aggregation. This approximation has also been applied to dense aggregates with spherical hull. The objective of this paper is to evaluate the effect of the non-sphericity on the rate constant of aggregation. We have specifically focused our study on the collision rate constant, i.e. assuming an aggregation efficiency coefficient equal to one. This follows the classical methodology being to distinguish collision dynamics and attachment kinetics. We will consider particles with a simple shape: sphere, discs, needles and spheroids. They have been selected to represent the whole of the precipitated particles and eventually lead to analytical calculations. We restrict ourselves to the collision induced by shear flow, which is the case for primary particles in particulate systems with Peclet number larger than 1, e.g. aqueous suspension of particles whose largest dimension is greater than 1µm. The ultimate goal of the article is to propose an approximate expression to the rate constant of collision; this relation will enable the numerical solving of a population balance equation, the particles being made up of objects with simple shapes, real or representative of more complex morphologies [34].

The paper is organized as follows: section 2 describes the tools and methods used to calculate the rate constant of collision. Section 3 presents the results corresponding to the collision of objects having the same shape, but homothetically different. Section 4 presents the results corresponding to the collision of particles with different shapes. Section 5 will discuss these results and conclude the paper.

2. Monte Carlo Simulations and statistics

Von Smoluchowski [2] has studied the collision between two spheres denoted 1 and 2 with different radii a_1 et a_2 moving in a shear flow with shear rate G. The corresponding rate constant K_{12} obeys the relation:

$$K_{12} = 4/3G\left(a_1 + a_2\right)^3 \qquad \text{Eq.1}$$

Along the calculation, the particle 1 is located at the origin of Cartesian coordinate system and is considered as motionless (see Figure 1). The particle 2 moves in the relative fluid flow with a straight trajectory parallel to the z axis (unit vector $\vec{k}$). The velocity is expressed as $\vec{V} = Gy\vec{k}$ in the Cartesian coordinate system $\left(\vec{i},\vec{j},\vec{k}\right)$. $\vec{j}$ is the unit vector in the direction of the shear (axis y). $\vec{i}$ is the unit vector in the direction perpendicular to $\vec{j}$ and $\vec{k}$ (axis x). $\vec{V}$ is also the velocity of the center of mass of the particle 2.

The flow is a pure shear flow just around the particle 1. It is, for instance, the case for particles moving in a turbulent flow. The initial orientation of the particle 2, i.e. close to the particle 1, is random. Then, a single particle in a shear flow undergoes a translation and rotation. For instance, in the case of a spheroidal particle, the end of the unit vector along the revolution axis follows circular (periodic) paths, called Jeffery trajectories [35]. The motion of the particle along these paths is unstable [36]. Moreover the relative motion of particles is made it more complicated by the presence of various physico-chemical interactions and interphase forces as drag, lift, hydrodynamic resistance [37]. Thus the actual trajectory should be estimated by means of computational fluid mechanics. As mentioned in the introduction, the usual practice is to include such phenomena in the aggregation efficiency. Considering only the collision rate and knowing that there is no favored orientation of non spherical particles at the beginning of the encounter, we will assume, as a rough approximation, that the orientation distribution of a single particle in a shear flow before the collision is uniform. This approach has to be considered as a first step in the search of simple kernel taking into account the asphericity of particles.

The objects considered in this paper are anisotropic, but have a center of symmetry and an axis of revolution. Each object is characterized by a triplet of values corresponding to three half-distances in a *3D* space (a_i,b_i,c_i) with $a_i \geq b_i \geq c_i$. The selected objects are the sphere (a_i,a_i,a_i), spheroids oblate (a_i,a_i,b_i) and prolate (a_i,b_i,b_i), disc (a_i,a_i,*0*) and needle (a_i,*0*,*0*).

The range of numerical values of K_{12}/G is very wide (see below). As K_{12}/G (in cubic meter) is roughly proportional to the particle size raised to the third power, scaling or normalization of K_{12} based on the expression of Von Smoluchowski ($=4/3G\left(X_1+X_2\right)^3$) appears to be relevant. X_i is a characteristic length of the object i. We denote $K_{12,N}\left(X_1,X_2\right)=K_{12}/\left[4/3G\left(X_1+X_2\right)^3\right]$. We have chosen for X_i a geometrical quantity related to the gyration radius $R_{g,i}$ for an ellipsoid and equal to $a_i=b_i=c_i$ for the sphere:

$$X_i=\sqrt{\left(a_i^2+b_i^2+c_i^2\right)/3} \qquad \text{Eq.2}$$

It can be underlined that the $X_i/R_{g,i}$ ratio remains constant for each object set (needles, discs, spheroids), each set having its own constant of proportionality. The anisotropy of a given object will be quantified by:

$$\lambda_i=X_i/a_i \qquad \text{Eq.3}$$

Then,

$$\lambda_1^N=1/\sqrt{3}<\lambda_1^P<\lambda_1^D<\lambda_1^O<\lambda_1^S=1$$

(S: sphere; O: spheroid oblate; D: disc; P: spheroid prolate; N: needle).

The collision of two objects is simulated by a Monte Carlo method with N_r runs, each one having the following steps:

One considers a cube with the edge a at the center of which is located the Cartesian coordinate system. The a value is taken equal to $4\times\max\left(a_1,a_2\right)$.

i. The particle 1 is located at the center of the coordinate system. Its orientation, i.e. orientation of the symmetry axis, is randomly selected.

ii. The particle 2, the orientation of which is randomly chosen too, is located inside the cube. Given four random numbers A_1, A_2, A_3 et A_4 within the [0 ;1] range, the coordinates of the center of the particle 2 are:

$$X_2=\left(2A_3-1\right)a/2$$

$$Y_2=\frac{2A_1-1}{\left|2A_1-1\right|}\sqrt{A_2}\,a/2$$

$$Z_2=\left(2A_4-1\right)a/2$$

The expression for *y*-coordinate of the particle 2 satisfies the likelihood of relative position between particles 1 and 2 in a shear flow [38].

iii. The particle shapes are projected onto the *xOy* plane perpendicularly to *Oz*. The figures generated by the projection are disc (for a sphere), line segment (for a needle), ellipse (for a disc or an ellipsoid).

iv. Any intersection between the projections of particles 1 and 2 is searched. The collision will be effective if the two projections overlap and if $Y_2 Z_2 < 0$. The latter condition means that the particle 2 is catching up with the particle 1 or is being caught up by particle 1: $Y_2 > 0\ Z_2 < 0$ or $Y_2 < 0\ Z_2 > 0$.

The collision rate constant is (*G=1*) :

$$K_{12} = \left(N_C / N_r \right) \left(a^3 / 2 \right) \qquad \text{Eq.4}$$

where N_C is the number of effective collisions. N_r is taken equal to 10^6, but may be modified in order to obtain the required accuracy (see below).

The considered particle pairs require to perform the calculation of the intersection between

i. two line segments

ii. a disc (or ellipse) and a line segment

iii. a disc (or ellipse) and another one

The two first cases can be analytically solved. The third one leads to the search of zeros of a quartic polynomial, for which the procedure of Rees has been used [39].

The above algorithm has been checked by comparing the Monte Carlo data to analytical calculations for the following object collisions: Sphere – Sphere (Eq.1), Sphere – Needle (appendix 1), Needle – Needle (appendix 2).

The algorithm performances have been estimated by performing twenty Monte Carlo calculations for a given pair of colliding objects. We have calculated the standard deviation σ and the mean value $\overline{K_{12,N}}$ for the sample, then the coefficient of variation $CV = \sigma / \overline{K_{12,N}}$, that is chosen as standard of calculation precision and repeatability. If the two objects are identical (shape and size), $0.006 < CV < 0.018$ $\left(N_r = 10^6 \right)$; *CV* is all the larger given the larger anisotropy of the object. If the objects have the same shape, but are differently sized, *CV* is all the larger given larger difference in size of the objects. N_r will be taken equal to 10^6 for spheroids oblate, discs and spheroids prolate (*b/a=c/a*>0.1); this is sufficient for getting a good repeatability ($CV < 0.04$) within a short computational time. In the case of more

anisotropic objects, the poorer performance needs to increase the value of N_r. For spheroid prolate with $b/a=c/a<0.1$, N_r will be taken equal to 10^7 ($CV < 0.04$). For needles, N_r will be taken equal to 3.10^7 ($CV < 0.04$). As shown in the appendix four, this choice restricts the modeling quality to $R^2<0.995$.

3. Collision between objects with same shape and different sizes

The collision rate constant has been calculated for the following pairs: sphere-sphere, oblate-oblate with various values of b_i/a_i (=0.5 ; 0.2), disc-disc, prolate-prolate with various values of b_i/a_i (=0.2 ; 0.05 ; 0.01), needle-needle. The impact of the ratio of the larger lengths (a_2/a_1) of the two particles has been studied within the range [10^{-2} ; 2.10^2].

The results are presented by taking the ratio ($h = X_2 / X_1$) in abscissa and $K_{12,N}$ in ordinate, more precisely $K_{12,N}^{i-i}\left(X_1, X_2\right) \quad i = \{1,2\}$. The superscript *i-i* expresses the collision between particles having the same shape. A dimensional analysis shows that $K_{12,N}^{i-i}\left(X_1, X_2\right)$ is a function of the single variable $h = X_2 / X_1$. Thus it may be written: $K_{12,N}^{i-i}\left(X_1, X_2\right) = K_{12,N}^{i-i}\left(h\right) \quad i = \{1,2\}$. For objets 1 and 2 with the same shape, but with different sizes, $h = a_2 / a_1 \neq 1$.

The figure 2 contains the data set (dots). The dashed lines represent the asymptotic value of $K_{12,N}^{i-i}$, i.e. when one particle is much larger than the other one. This asymptotic value, denoted $K_{12,N}^{i-i}\left(0\right)$, can be obtained by considering the collision between a point-like particle (particle 2) and the particle 1. The analytical calculation of the corresponding $K_{12,N}$ is reported in the appendix 3.

A first analysis of the curves shows that:

- More anisotropic are the colliding particles, smaller is the $K_{12,N}$ value
- If the colliding particles have the same size, $K_{12,N}$, denoted $K_{12,N}^{i-i}\left(1\right)$, has a value within the [0.308; 1] range. The value for the most anisotropic particles (needles) is not so small.
- More different in size are the colliding particles, smaller is the $K_{12,N}$ value. This variation is all larger given the larger anisotropy factor of the particles.
- The asymptotic value is non-zero for all objects except for the needles.

Table 1 contains the $K_{12,N}^{i-i}(0)$ values got from analytical calculation and the $K_{12,N}^{i-i}(1)$ values got from Monte Carlo calculation, for objects with various shapes.

The $K_{12,N}$ value depends on the anisotropy factor λ of the two objects and on their ratio h of homothety.

i. If the objects are identical, i.e. $h=1$, $K_{12,N}^{i-i} = K_{12,N}^{i-i}(1)$ only depends on the mutual anisotropy.

ii. If one of the two objects is point-like, i.e. $h=0$ or $h \to \infty$, $K_{12,N}^{i-i} = K_{12,N}^{i-i}(0) = K_{12,N}^{i-i}(\infty)$ only depends on the anisotropy of the larger object.

iii. If the two objects are not identical ($h \neq 1$), the symmetry of the problem with respect to the exchange of the two colliding objects requires that any model should be invariant by the transform $h \to h^{-1}$.

Therefore, it makes sense to look for such an expression:

$$K_{12,N}^{i-i}(h) = K_{12,N}^{i-i}(0) + g(h)\left(K_{12,N}^{i-i}(1) - K_{12,N}^{i-i}(0)\right) \quad \text{Eq.5}$$

with the following requirements (R1, R2, R3):

$$g(h) = g\left(h^{-1}\right) \quad \text{(R1)}$$

$$g(1) = 1 \quad \text{(R2)}$$

$$g(\infty) = g(0) = 0 \quad \text{(R3)}$$

A function fulfilling these conditions is:

$$g(h) = \left[\left(h^m + h^{-m}\right)/2\right]^{-p} \quad \text{Eq.6}$$

We have performed a fitting of Monte Carlo data reported in the figure 2 by using the least square method with (*m*,*p*) as parameters and the minimization of the root mean square error (*RMSE*) as criteria. The best model ($RMSE = 0.017$; $R^2 = 0.998$) is obtained for the values of exponents m=0.36 and p=3.

It can be underlined that the agreement between the model (Eqs.5-6) and the data is as good if the two exponents are linked by the relation $p \times m^{1.68} = 0.54 \quad \forall p > 2.5$.

The application of equations 5-6 is reported on figure 2 (solid line).

The previous results show the relevance of the choice of the X_i expression (Eq.2) for the objects set. We emphasize that the disc has a gyration radius ($R_g = a/\sqrt{2}$) different from the

one of the spheroid oblate with $b_i/a_i<<1$ ($R_g = \sqrt{2/5}\,a$), whereas their respective K_{12} and X_i ($=\sqrt{2/3}\,a$) are equal.

4. Collision between objects with different shape and size

The collision rate constant has been computed for the following pairs: sphere-disc, sphere-prolate, sphere-needle, disc-needle. The results are presented in the Figure 3 by taking the ratio h ($h = X_2 / X_1 \neq a_2 / a_1$) as abscissa and $K_{12,N}$ as ordinate. We can see that:

- If one of the two particles is much smaller than the other one, the former may be considered as a point-like particle; the asymptotic $K_{12,N}$ value (appendix 3) is the same that the one computed for the collision between objects with the same shape (Figure 2). This is observed for both $h \to 0$ et $h \to \infty$.
- One deduces that the curves contain information about the larger object if $h \to 0$ et $h \to \infty$

These results suggest that the corresponding data may be represented by means of a composition law:

$$K_{12,N}^{1-2}(h) = f(h)\,K_{12,N}^{1-1}(h) + f\left(h^{-1}\right)K_{12,N}^{2-2}\left(h^{-1}\right) \qquad \text{Eq.7}$$

f is a function of h. $K_{12,N}^{i-j}(h)$ is the dimensionless rate constant of collision between the objects i and j (i, j in $\{1,2\}$), with different shapes ($i \neq j$) or same shape ($i = j$) and size ratio h. The equation 7 and the function f must meet the following conditions (C1, C2, C3):

$$h \to 0 \quad f(h) \to 1 \quad K_{12,N}^{1-2} \to K_{12,N}^{1-1}(0) \qquad \text{(C1)}$$

$$h \to \infty \quad f(h) \to 0 \quad K_{12,N}^{1-2} \to K_{12,N}^{2-2}(0) \qquad \text{(C2)}$$

If the colliding particles have the same shape, then:

$$K_{12,N}^{1-2}(h) = f(h)\,K_{12,N}^{i-i}(h) + f\left(h^{-1}\right)K_{12,N}^{i-i}\left(h^{-1}\right) = K_{12,N}^{i-i}(h) \quad i = 1,2 \qquad \text{(Eq.8)}$$

which imposes (see iii. in section 3):

$$f\left(h^{-1}\right) = 1 - f(h) \qquad \text{(C3)}$$

Thus, the expression (Eq.9) would be a good candidate meeting these requirements (C1, C2):

$$f(h) = \frac{1}{1+h^n} \qquad \text{Eq.9}$$

We have performed a fitting of a model consisting in Equations 7 and 9 with the Monte Carlo data by using the least square method with *n* as parameter and the minimization of the root mean square error (*RMSE*) as criteria. The $K_{12,N}^{i-i}(h)$ values are those calculated by the Monte Carlo method and presented in the section three. The optimal value for *n* is found equal to *n*=1.3 ($RMSE = 0.022$; $R^2 = 0.996$). The figure 3 compares the model (dotted lines) and the Monte Carlo calculations (dots).

5. Discussion and conclusion

Along the sections 3 and 4, we have considered separately the collisions of objects with the same shape and different shapes. Two separate and independent models have been provided. Now, we consider the use of equations 5-9 for the calculation of $K_{12,N}^{i-j}(h)$. $K_{12,N}^{i-j}(h)$ obeys therefore the expression:

$$K_{12,N}^{1-2}(h) = \frac{1}{1+h^n}\left(K_{12,N}^{1-1}(0) + \left[\left(h^m + h^{-m}\right)/2\right]^{-p}\left(K_{12,N}^{1-1}(1) - K_{12,N}^{1-1}(0)\right)\right) + \frac{1}{1+h^{-n}}\left(K_{12,N}^{2-2}(0) + \left[\left(h^m + h^{-m}\right)/2\right]^{-p}\left(K_{12,N}^{2-2}(1) - K_{12,N}^{2-2}(0)\right)\right) \quad \text{Eq.10}$$

The model contains three parameters: *n*, *m* and *p*. The optimal values of the exponents *m*, *p* and *n* are taken equal to 0.36, 3 and 1.30, values already determined in the sections 3-4. We note in the figure 3 that the agreement between the Monte Carlo data (dots) and the model (solid line) is very good. The root mean square error is $RMSE = 0.015, R^2 = 0.998$.

However the model needs the knowledge of $K_{12,N}^{i-i}(0)$ and $K_{12,N}^{i-i}(1)$, the values of which are obtained from analytical calculations and Monte Carlo calculations respectively. These quantities depend on the shape parameters, *k=b/a* and *l=c/a*, that are the same for the two colliding particles. It is interesting to express $K_{12,N}^{i-i}(0)$ and $K_{12,N}^{i-i}(1)$ as an approximate function of these shape parameters. In view of the form of equations 5 and 10, we will consider thereafter the functions

$$P(k,l) = K_{12,N}^{i-i}(0) \quad \text{Eq.11a}$$

$$Q(k,l) = K_{12,N}^{i-i}(1) - K_{12,N}^{i-i}(0) \quad \text{Eq.11b}$$

Having no theoretical model for these functions, we logically search for each function a linear combination of polynomials in *k* and *l*:

$$P(k,l) = \sum_j P_j f_j(k,l) \qquad \text{Eq.12a}$$

$$Q(k,l) = \sum_j Q_j f_j(k,l) \qquad \text{Eq.12b}$$

The functions *P*, *Q* and f_j must be invariant under the exchange of *k* and *l*. The functions set $\{ f_j(k,l) \}$ is infinite and the selected sub-set is just limited by the authors creativity. We have chosen the following set:

$$f_{j=0..10} = \left\{1, \frac{k+l}{2}, \frac{k^2+l^2}{2}, kl, \left(\frac{k+l}{2}\right)^2, \frac{k^3+l^3}{2}, kl\left(\frac{k+l}{2}\right), \left(\frac{k+l}{2}\right)^3, \frac{k^4+l^4}{2}, (kl)^2, \left(\frac{k+l}{2}\right)^4\right\}$$

Eq.13

P_j et Q_j are the coefficients to be determined. It should be noted that $K_{12,N}^{i-i}(X_1, X_2) = 1 \; \forall X_1, X_2$ for the collision of two spheres, i.e. $P(1,1) = 1; Q(1,1) = 0$. We deduce the relationship between the coefficients:

$$\sum_j P_j = 1 \qquad \text{Eq.14a}$$

$$\sum_j Q_j = 0 \qquad \text{Eq.14b}$$

The analytical value of $K_{12,N}^{i-i}$ for two needles (*k*=*l*=0) with the same length being 0.3084, the following expression is valid as well:

$$P_0 + Q_0 = 0.3084 \qquad \text{Eq.15}$$

It is known that the consideration of a large number of $f_j(k,l)$ functions for fitting data and model improves the coefficient of determination R^2 but leads to two major drawbacks:

- the increase of the risk to build a fortuitous model [40]
- a decrease of the model predictability.

The best model corresponding to equations 12a,b has been searched by using the optimization of the predictive R^2: Q^2 in a cross validation method using the leave-one-out scheme. This approach, similar to the one used in another study [41], is depicted in appendix 4. It leads to a predictive and parcimonious model. It appears that a model with four parameters is sufficient

to reproduce the values calculated by the Monte Carlo method with an accuracy consistent with the one of the Monte Carlo calculations. The selected functions are: $\left\{1, \frac{k+l}{2}, \left(\frac{k+l}{2}\right)^3, (kl)^2\right\}$.

$$P(k,l) = P_0 + P_1 \frac{k+l}{2} + P_2 \left(\frac{k+l}{2}\right)^3 + P_3 (kl)^2 \qquad \text{Eq.16a}$$

$$Q(k,l) = Q_0 + Q_1 \frac{k+l}{2} + Q_2 \left(\frac{k+l}{2}\right)^3 + Q_3 (kl)^2 \qquad \text{Eq.16b}$$

The parameter values of the model leading to the best fit are reported in the Table 2.

To test the model, we have considered the two object pairs: P0.05-N and P0.2-N, that have not been involved for the building of the model. Then, we have calculated $K_{12,N}^{1-2}(h)$ by using the Monte Carlo method and compared these data to the ones coming from the model (Figure 4). The model is based on the equations 10 and 16a-b. We see that the model is in good agreement with the data coming from the Monte Carlo calculations (P0.05-N : *RMSE*=0.0086, R^2=0.994 ; P0.2-N : *RMSE*=0.0075, R^2=0.9984). (see Table 3).

To conclude, we have calculated by using Monte Carlo simulations, the rate constant or kernel of collision between particles with simple shapes, but with various anisotropy factors, in a shear flow. These data were used to build an empirical analytical model for the collision rate constant. Any object is characterized by three internal distances in three mutually perpendicular directions. The model is expressed as a formula including the six internal distances and the shear rate as well. It describes very reasonably the data coming from Monte Carlo calculations. All the objects used for the building of the model have a center of symmetry and an axis of symmetry at least. One can ask whether the model would remain valid for objects described by three internal distances, but without the above-mentioned properties of symmetry. The results obtained in this paper are the starting point of a study undertaken to answer this question.

References

[1] M.V. Smoluchowski, Drei Vorträge über Diffusion, Brownsche Bewegung und Koagulation von Kolloidteilchen, Zeitschrift Für Physik. 17 (1916) 557–585.

[2] M.V. Smoluchowski, Versuch einer mathematischen Theorie der Koagulationskinetik kolloider Lösungen, Z. Physik. Chem. 92 (1917) 129-168

[3] P.G. Saffman and J.S. Turner, On the collision of drops in turbulent clouds, J. Fluid Mech., 1(1956)16-30.

[4] C. Oh and C.M. Sorensen, Light scattering study of fractal cluster aggregation near the free molecular regime, J. Aerosol Sci., 28(1997)937-957

[5] E.J.W Verwey .and J.T.G. Overbeek, " Theory of the Stability of Lyophobics Colloids ", Elsevier, Amsterdam (1948).

[6] M. Elimelech, J. Gregory, X. Jia, R. Williams, Particle deposition & aggregation, Butterworth-Heinemann, 1995

[7] N. Fuchs, Ueber die Stabilität und Aufladung der Aerosole, Z. Phys. 89(1934)736-743

[8] L. A. Spielman, Viscous interactions in Brownian coagulation, J. Colloid and Interface Sci., 33(1970)562-571.

[9] G.R. Zeichner and W.R. Schowalter, Use of trajectory analysis to study stability of colloidal dispersions in flow fields, AIChE J. 23(1977)243-254

[10] O.I. Vinogradova, Coagulation of hydrophobic and hydrophilic solids under dynamic conditions, J. Colloid and Interface Sci., 169 (1995) 306-312.

[11] Y. Adachi, M.A. Cohen Stuart and R. Fokkink, Kinetics of turbulent coagulation studied by means of end-over-end rotation, J. Colloid and Interface Sci., 165(1994)310-317

[12] F. Gruy, Formation of small silica aggregates by turbulent aggregation, J. Colloid and Interface Sci, 237(2001) 28-39

[13] P. Meakin, Formation of Fractal Clusters and Networks by Irreversible Diffusion-Limited Aggregation, Phys. Rev. Lett. 51 (1983) 1119–1122.

[14] R. Jullien, The application of fractals to colloidal aggregation, Croatica Chemica acta 65(1992)215-235

[15] F. Family and D.P. Landau, Kinetics of aggregation and gelation, North-Holland, 1984

[16] F. Babick, Suspension of colloidal particles and aggregates, Particle Technology Series, Springer, 2016.

[17] S. Veerapaneni, M.R. Wiesner, Hydrodynamics of fractal aggregates with radially varying permeability, J. Colloid and Interface Sci., 177 (1996) 45-57.

[18] K.A. Kusters, J.G.Wijers, D.Thoenes, Aggregation kinetics of small particles in agitated

vessels, Chem. Eng. Sci., 52 (1997)107-121

[19] Y. Xiong and S.E. Pratsinis, Formation of agglomerate particles by coagulation and sintering: Part1: a two-dimensional solution of the population balance equation, J. Aerosol Sci., 24(1993)283-300

[20] G. Yang and P. Biswas, Computer simulation of the aggregation and sintering restructuring of fractal-like clusters containing limited numbers of primary particles, J. Colloid and Interface Sci., 211(1999)142-150

[21] M. Soos, J. Sefcik, M. Morbidelli, Investigation of aggregation, breakage and restructuring kinetics of colloidal dispersions in turbulent flows by population balance modelling and static light scattering, Chem. Eng. Sci., 61(2006)2349-2363

[22] M. Kostoglou, A.G. Konstandopoulos, S.K. Friedlander, Bivariate population dynamics simulation of fractal aerosol aggregate coagulation and restructuring, Aerosol Sci. 37(2006)1102-1115

[23] C. Selomulya, R. Amal, G. Bushell, T.D. Waite, Evidence of shear rate dependence on restructuring and breakup of latex aggregates, J. Colloid and Interface Sci., 236(2001)67-77

[24] L. Gmachowski, Aggregate restructuring and its effect on the aggregate size distribution, Colloids and surfaces, A: Physicochemical and Engineering Aspects 207(2002)271-277

[25] M.L. Eggersdorfer, Nanoparticle agglomerates and aggregates in aerosols by coagulation and sintering, PhD Thesis, ETH Zürich, 2012.

[26] F.Gruy, Modelling of aggregate restructuring in a weakly turbulent flow, Colloids and surfaces, A: Physicochemical and Engineering Aspects 395(2012)54-62

[27] S.K. Friedlander and C.S. Wang, The self-preserving particle size distribution for coagulation by Brownian motion, J. Colloid and Interface Sci., 22(1966)126-132

[28] A.A. Lushnikov, Evolution of coagulating systems, J. Colloid and Interface Sci., 45(1973)549-556

[29] E. Rückenstein and B. Pulvermacher, Kinetics of crystallite sintering during heat treatment of supported metal catalysts, AIChE J. 19(1973)356-364

[30] E. Matijevic, Monodispersed colloids: art and science, Langmuir. 2 (1986) 12–20.

[31] T. Sugimoto, Monodispersed Particles, Elsevier, 2001.

[32] J.C. Loudet, A.M. Alsayed, J. Zhang and A.G. Yodh, Capillary interactions between anisotropic colloidal particles, PRL 94,018301 (2005).

[33] S. Bounoua, E. Lemaire, J F_erec, G Ausias, P Kuzhir. Shear-thinning in concentrated rigid fiber suspensions: Aggregation induced by adhesive interactions. Journal of Rheology, American Institute of Physics, 60(2016)1279-1300. <10.1122/1.4965431>. <hal-01422136>

[34] F. Gruy, Inertia tensor as morphological descriptor for aggregation dynamics, Colloids and Surfaces A: Physicochemical and Engineering Aspects. 482 (2015) 154–164.

[35] G.B. Jeffery, The Motion of Ellipsoidal Particles Immersed in a Viscous Fluid, Proceedings of the Royal Society of London A: Mathematical, Physical and Engineering Sciences. 102 (1922) 161–179.

[36] M.S. Ingber and L.A. Mondy, A numerical study of three-dimensional Jeffery orbits in shear flow, J. of Rheology 38 (1994) 1829-1843.

[37] J.S. Marshall and S. Li, Adhesive particle flow: a discrete-element approach, Cambridge University Press, N.Y., USA, 2014.

[38] C. Walck, Handbook on statistical distributions for experimentalists, internal report SUF-PFY, Stockholm, 2007

[39] E.L. Rees, Graphical Discussion of the Roots of a Quartic Equation, The American Mathematical Monthly. 29 (1922) 51–55.

[40] N. Verzelen, Minimax risks for sparse regressions: Ultra-high-dimensional phenomenons, Electronic Journal of Statistics. 2012 (2010) 38–90.

[41] P. Nortier, P. Chagnon, A.E. Lewis, Modelling the solubility in Bayer Liquors: a critical review and new models, Chemical Engineering Science. 66 (2011) 2596–2605.

[42] H. Wold, Soft modeling: The basic design and some extensions, in: Systems Under Indirect Observation: Causality Structure, Prediction, North-Holland, Amsterdam, 1982: pp. 1–54.

[43] N.T. Quan, The Prediction Sum of Squares as a General Measure for Regression Diagnostics, Journal of Business and Economic Statistics. 6 (1988) 501–504.

Appendix 1: K_{12} for the collision between a needle with length L and a sphere with radius R

The general expression for the rate constant (kernel) of collision between two particles with any shape in a shear flow is, following Von Smoluchowski [2]:

$$K_{12}^{O1,O2} = \int_{P_{\vec{k},K_1} \cap P_{\vec{k},K_2} \neq \varnothing} G \left| \overrightarrow{C_1 C_2} \bullet \vec{j} \right| d\sigma_{P,\overrightarrow{C_1 C_2}} \qquad \text{A1-1}$$

$$K_{12} = \left\langle K_{12}^{O1,O2} \right\rangle_{O_1,O_2} \qquad \text{A1-2}$$

C_1 and C_2 are the centers of mass of the colliding objects 1 and 2. K_1 and K_2 are the objects 1 and 2 consisting of geometrical points (see Figure 1). $P_{\vec{k},K_i}$ is the projection of K_i onto the plane perpendicular to the vector $\vec{k}$. $W = P_{\vec{k},K_1} \cap P_{\vec{k},K_2}$ is the intersection of the projections of K_1 and K_2 onto the plane perpendicular to $\vec{k}$. $d\sigma_{P,\overrightarrow{C_1 C_2}}$ is the infinitesimal area element, in the plane of projection, around the center of mass of the object 2 (1 being the reference particle). $\langle \ \rangle_{O_1,O_2}$ is the average over all the orientations O_1 and O_2 for objects 1 and 2.

One calculate by using the same methodology as for the collision of two spheres the contribution $K_{12}^{O1,O2}$ of a given needle orientation to K_{12} (orientation of the sphere is trivial). The needle orientation is characterized by the angles θ and ϕ. θ is the angle between the needle projection onto the *xOy* plane and the *x'Ox* axis. ϕ is the angle between the needle and the *Oz* axis. The length of the needle projection is $L_p = L\sin\phi$. Two cases may occur:

- $L_p / 2\sin\theta > -R\cos\theta$

thus

$$K_{12}^{O1,O2} / G = L_p R^2 \frac{\pi}{2}\sin\theta + \frac{2}{3}R^3\left(\sin\theta + 1/\sin\theta\right) + \frac{1}{2}RL_p^2\sin\theta \qquad \pi/2 \le \theta \le \pi \qquad \text{A1-3}$$

- $L_p / 2\sin\theta < -R\cos\theta$

thus

$$K_{12}^{O1,O2}/G = L_p R^2 \sin\theta\left(\pi-\theta+Arc\sin\left(\frac{L_p\sin\theta}{2R}\right)\right)-L_p\cos\theta\left(R^2+\frac{1}{12}L_p^2\sin^2\theta\right) \qquad \pi/2\le\theta\le\pi$$
$$+4/3\left(R^2+\frac{1}{8}L_p^2\sin^2\theta\right)\left(R^2-\frac{1}{4}L_p^2\sin^2\theta\right)^{1/2}$$

A1-4

K_{12} is the average of $K_{12}^{O1,O2}$ over all the needle orientations (the average simply applies to the sphere) :

$$K_{12}=\frac{2}{\pi}\iint_{\theta\in[\pi/2,\pi],\phi\in[0,\pi/2]} K_{12}^{O1,O2}(\phi,\theta)\sin\phi d\phi d\theta \qquad \text{A1-5}$$

Appendix 2: K_{12} for the collision between two needles with lengths L_1 and L_2 repectively

The orientation of each needle is characterized by the angles θ_i and ϕ_i. θ_i is the angle between the projection of needle i ($=\{1,2\}$) onto the xOy plane and the $x'Ox$ axis. ϕ_i is the angle between the needle i and the Oz axis. The length of the needle projection is $L_{p,i} = L_i \sin\phi_i$. Two cases may occur ($0 \le \theta_2 < \theta_1 \le \pi$):

- $L_{p1} / 2\sin\theta_1 > L_{p2} / 2\sin\theta_2$

thus

$$K_{12}^{O1,O2} / G = \frac{2}{3}\left|\tan^{-1}\theta_2 - \tan^{-1}\theta_1\right|\left(L_{p,2} / 2\sin\theta_2\right)\left(\left(L_{p,2} / 2\sin\theta_2\right)^2 + 3\left(L_{p,1} / 2\sin\theta_1\right)^2\right) \qquad \text{A2-1}$$

- $L_{p1} / 2\sin\theta_1 < L_{p2} / 2\sin\theta_2$

thus

$$K_{12}^{O1,O2} / G = \frac{2}{3}\left|\tan^{-1}\theta_2 - \tan^{-1}\theta_1\right|\left(L_{p,1} / 2\sin\theta_1\right)\left(\left(L_{p,1} / 2\sin\theta_1\right)^2 + 3\left(L_{p,2} / 2\sin\theta_2\right)^2\right) \qquad \text{A2-2}$$

K_{12} is the average of $K_{12}^{O1,O2}$ over all the orientations of the two needles:

$$\begin{aligned} K_{12} = {} & \frac{1}{2\pi^2} \iint\limits_{\theta_1 > \theta_2 \in [0,\pi]^2, \phi_1, \phi_2 \in [0,\pi/2]^2} K_{12}^{O1,O2}\left(\phi_1, \theta_1, \phi_2, \theta_2\right) \sin\phi_1 d\phi_1 d\theta_1 \sin\phi_2 d\phi_2 d\theta_2 \\ & + \frac{1}{2\pi^2} \iint\limits_{\theta_1 < \theta_2 \in [0,\pi]^2, \phi_1, \phi_2 \in [0,\pi/2]^2} K_{12}^{O1,O2}\left(\phi_2, \theta_2, \phi_1, \theta_1\right) \sin\phi_1 d\phi_1 d\theta_1 \sin\phi_2 d\phi_2 d\theta_2 \end{aligned} \qquad \text{A2-3}$$

Appendix 3: K_{12} for the collision between a spheroid and a point-like particle

- **prolate (a_1,b_1,b_1)**

$$K_{12}^{O1,O2}/G=\frac{4}{3}a_p b_p\sqrt{\left(b_p\cos\theta_1\right)^2+\left(a_p\sin\theta_1\right)^2} \qquad \text{A3-1}$$

a_p and b_p are the lengths of semi-axes of the spheroid projection, i.e. an ellipse, on a plane perpendicular to the flow direction:

$$a_p=\sqrt{\left(b_1\cos\phi_1\right)^2+\left(a_1\sin\phi_1\right)^2}$$
$$b_p=b_1$$

The axis of revolution of the spheroid (prolate and oblate) is characterized by the angles θ and ϕ. ϕ is the angle between the axis of revolution and the *Oz* axis. θ is the angle between the axis projection onto the *xOy* plane and the *x'Ox* axis.

- **oblate (a_1,a_1,b_1)**

$$K_{12}^{O1,O2}/G=\frac{4}{3}a_p b_p\sqrt{\left(b_p\sin\theta_1\right)^2+\left(a_p\cos\theta_1\right)^2} \qquad \text{A3-2}$$

with

$$a_p=a_1$$
$$b_p=\sqrt{\left(b_1\sin\phi_1\right)^2+\left(a_1\cos\phi_1\right)^2}$$

endly,

$$K_{12}=\frac{1}{\pi}\iint\limits_{\theta_1\in[0,\pi],\phi_1\in[0,\pi/2]}K_{12}^{O1,O2}\left(\phi_1,\theta_1\right)\sin\phi_1 d\phi_1 d\theta_1 \qquad \text{A3-3}$$

and

$$K_{12,N}=K_{12}/\left(4/3G\,a_1^3\lambda_1^3\right) \qquad \text{A3-4}$$

if $b_1 \to 0$, then $K_{12,N} \to \frac{4}{3\pi} 3^{3/2} \frac{b_1}{a_1}$ (prolate) and $K_{12,N} \to (3/2)^{3/2} \frac{4}{3\pi}$ (oblate)

Appendix 4: Details of statistical calculations and modeling procedures

Precision of the Monte Carlo calculations of $K_{12,N}$ (section 2): for each couple of objects considered, a sample of 20 independent observations ((y_i), i∈{1,…I}, I = 20) was calculated by repeating the described Monte-Carlo procedure with independent random draws. As usual, the sample mean $\overline{y_s}$,the sample standard deviation σ_s and the (sample) coefficient of variation *CV* are calculated according to : $\overline{y_s} = \frac{1}{I}\sum_{i=1}^{I} y_i$, $\sigma_s = \sqrt{\frac{1}{I-1}\sum_{i=1}^{I}\left(y_i - \overline{y_s}\right)^2}$, $CV = \sigma_s / \overline{y_s}$

Limitation of the quality of models due to the error in MC calculations

A model cannot be better than the data it represents. To check the effect of *CV* = 0.04 on the maximum R^2 that can be obtained in any model, we performed this calculation using Matlab and the set of data for $K_{12,N}$ depicted in figure 2 $y_{k1} = K_{12,N,k1}$: generate a normal distribution of *k.l* random values r_{kl} **((***k,l***)**∈{1,6}x{1,15}) with mean =1 and standard deviation 0.04, generate a "noisy" set of values $y_{kl} = y_{kl} \otimes r_{kl}$ and calculate the value of R^2 corresponding according to $R^2 = 1 - \sum_{k=1}^{6}\sum_{l=1}^{15}\left(y_{kl} - y_{kl}\right)^2 / \sum_{k=1}^{6}\sum_{l=1}^{15}\left(y_{kl} - \overline{y}\right)^2$. The average value of R^2 on 10000 draws is 0.995. This result suggests that any model with $R^2 \geq 0.995$ can be considered as having its accuracy limited by the precision of the data to be modeled.

Fitting procedure, least square method, section 3, model from Eqs.5-6:

For each pair *k* (*k*∈{1,6}) of identical form objects, $K_{12,N,k}^{i-i}(1)$ is known from the MC calculation at *h*=1 and $K_{12,N,k}^{i-i}(0)$ from the analytical calculation described in Appendix 3. Each point *l* (*l*∈{1,15}), ($K_{12,N,k,l}^{i-i} = y_{kl}, h_l$) on the corresponding curve is modelled according to Eqs. 5-6 : $y_{kl} = K_{12,N,k}^{i-i}(0) + \left[\left(h_l^m + h_l^{-m}\right)/2\right]^{-p}\left(K_{12,N,k}^{i-i}(1) - K_{12,N,k}^{i-i}(0)\right)$ using a Microsoft Excel worksheet.

For all points ((*k,l***)**∈{1,6}x{1,15}), *m* and *p* are kept identical, the Sum of Squared Errors (*SSE*) is calculated according to : $SSE = \sum_{k=1}^{6}\sum_{l=1}^{15}\left(y_{kl} - y_{kl}\right)^2$; the Solver add_in in Excel is then

used with *SSE* as the "Objective" cell and *m* and *p* as the "Variable" cells to determine the values of *m* and *p* than yield the minimum value of *SSE*. These values are: *m* = 0.36 and *p* = 3.0.

Fitting procedure, least square method, section 4, model from Eqs. 7-9:

The procedure is basically the same as for the model in §3, Eqs. 5-6, but the points $K_{12,N,k,l}^{i-j} = y_{kl}, h_l$ are those depicted in figure 3, y_{kl} related to the point *l* on the set from the pair of objects *k* ((k,l)∈{1,5}x{1,15}) . The values of $K_{12,N,k}^{1-1}\left(h_l\right)$ and $K_{12,N,k}^{2-2}\left(1/h_l\right)$ are those from the MC calculation. The equation for the model is $y_{kl} = \frac{1}{1+h_l^n} K_{12,N,k}^{1-1}\left(h_l\right) + \frac{h_l^n}{1+h_l^n} K_{12,N,k}^{2-2}\left(1/h_l\right)$. The value of *n* is kept identical for all points, *n* is the "Variable" cell for the solver. *SSE* is found minimal when *n* = 1.3.

Verification procedure, least square method, section 5, model from Eq. 10:

As in the fitting procedure, section 4, Eqs. 7-9, the observed values are those of figure 3 and the model is: $y_{kl} = \frac{1}{1+h_l^n} K_{12,N,k}^{1-1}\left(h_l\right) + \frac{h_l^n}{1+h_l^n} K_{12,N,k}^{2-2}\left(1/h_l\right)$, with this modification: the values of $K_{12,N,k}^{i-i}\left(h_l\right)$ are not taken from the MC calculation, but from the model of section 3, Eqs. 5-6: $K_{12,N,k}^{i-i}\left(h_l\right) = K_{12,N,k}^{i-i}\left(0\right) + \left[\left(h_l^m + h_l^{-m}\right)/2\right]^{-p}\left(K_{12,N,k}^{i-i}\left(1\right) - K_{12,N,k}^{i-i}\left(0\right)\right)$. The values of *m*, *n* and *p* are kept at the optimal values determined before (resp. 0.36, 1.3 and 3.0). The Root Mean Square Error (*RMSE*) and R^2 are classically calcutated according to: $RMSE = \sqrt{SSE/N}$ where *N* is the total number of observations (5*15=75) and $R^2 = 1 - SSE / \sum_{k=1}^{5}\sum_{l=1}^{15}\left(y_{kl} - \bar{y}\right)^2$

Modelling, section 5, Eq. 16a-b

Let us first remark that this modeling does not have any physical basis but is necessary in the framework of the use of K_{12} in Population Balance Equations (PBE) where computing load is critical. Consequently, the MC calculation of $K_{12,N,k}^{i-i}\left(1\right)$ is too slow, as even is the numerical evaluation of the integral in the calculation of $K_{12,N,k}^{i-i}\left(0\right)$ (A3-3).

The hypothesis and constraints of this modelling were:

- $P(k,l) = K_{12,N}^{i-i}(0)$ and $Q(k,l) = K_{12,N}^{i-i}(1) - K_{12,N}^{i-i}(0)$ are functions of *k* and *l* only
- *P(k,l)* and *Q(k,l)* are not modified by the exchange of *k* and *l*
- *P(1,l)* = 1, *Q(1,1)* = 0 (case of a sphere)
- for identical needles where *h*=1: $K_{12,N}^{i-i}(1)$ =0.3084, consequently, according to Eq. 10: 0.3084 = *P(0,0)+Q(0,0)*

For the sake of simplicity, we first searched a solution as a linear combination of simple functions of *k* and *l*, respecting the invariance by exchange, as the 11 functions:

$$f_{j=0..10} = \left\{1, \frac{k+l}{2}, \frac{k^2+l^2}{2}, kl, \left(\frac{k+l}{2}\right)^2, \frac{k^3+l^3}{2}, kl\left(\frac{k+l}{2}\right), \left(\frac{k+l}{2}\right)^3, \frac{k^4+l^4}{2}, (kl)^2, \left(\frac{k+l}{2}\right)^4\right\}$$

This list was only limited by our creativity but revealed to contain a set of functions that correctly reach the objective.

The data to be modelled (observations) are issued from the 7 values in table 1 for each of the responses *P* and *Q*.

With 7 observations and 11 candidate predictors, the ensemble of solutions is infinite; any subset of 7 predictors would yield a "perfect" model in terms of explanation of the variance (R^2=1). However, these models would have no predictive capacity for values of (*k*,*l*) not in the set described by the 7 objects in table 1. Moreover, Verzelen [40] showed that incorporating too many predictors in a model drastically increases the risk to build a fortuitious model. Consequently, we decided to limit the number of predictors in the model to the minimum necessary to build a model with a level of quality equal to the maximum consistent with the accuracy of the MC calculations, namely R^2 =0.995. The choice of the best subset was based on a procedure similar to the one used by Nortier & al. [41] Because R^2 can only increase with the addition of one more predictor in the model, the criteria for the model selection was the predictive R^2, or Q^2 introduced by Wold [42] and refined by Quan [43]. In short, this is a cross validation method using the leave-one-out scheme. Contrary to [41], the authors programmed in this work the whole scheme in Matlab, with the multi-linear regression based on Matlab's function "regress".

The Q^2 criteria was calculated for all combinations of "1" plus up to 4 functions in the 10 non constant candidate predictors, for both *P* and *Q* responses. In both cases (*P* or *Q*), the best set of "1" plus 3 non constant predictors was: *1, (k+l)/2, ((k+l)/2)*^{3}*, (kl)*^{2}, with Q^2 = 0.9993 and R^2 = 1.000 for *P* and Q^2 = 0.9984 and R^2 = 0.9998 for *Q*, which satisfies our criteria.

Due to intrinsic features of Matlab function "regress", the above described calculation could not take the constraints on *P(1,1)*($P_0 = 1-(P_1+P_2+P_3)$), *Q(1,1)*($Q_1 = -(Q_0+Q_2+Q_3)$) and *P(0,0)* + *Q(0,0)*($Q_0 = 0.3084 - P_0$) into account: so, once the best model was obtained, we made another multilinear regression with the Matlab function "regress" the considering 5 variables P_1, P_2, P_3, Q_2 and Q_3 and the equations:

$$P(k,l)-1 = P_1\left(\frac{k+l}{2}-1\right)+P_2\left(\left(\frac{k+l}{2}\right)^3-1\right)+P_3\left((kl)^2-1\right)$$

$$Q(k,l)-0.3084\left(1-\frac{k+l}{2}\right) = Q_2\left(\left(\frac{k+l}{2}\right)^3-\frac{k+l}{2}\right)+Q_3\left((kl)^2-\frac{k+l}{2}\right)$$

The resulting values are given in table 2 and provide $RMSE_P$ = 0.0047, R^2_P = 0.9999, $RMSE_Q$=0.0027, R^2_Q = 0.9996.

Figure captions

Figure 1: Sketch of the collision between two particles moving in a shear flow.

Figure 2: dimensionless rate constant of collision $K_{12,N}$ as a function of $h=X_2/X_1$ ratio for various pairs Y-Y of particles with the same shape Y (S: sphere; O b/a: spheroid oblate with b/a ratio; D: disc; P b/a: spheroid prolate with b/a ratio; N: needle)
dots: Monte Carlo calculation
dashed line (--): asymptotic value of $K_{12,N}$
solid line: model (Eqs.5-6)

Figure 2 (zoom)

Figure 3: dimensionless rate constant of collision $K_{12,N}$ as a function of $h=X_2/X_1$ ratio for various pairs of particles with different shapes: D-S, S-P 0.2, S-P 0.05, S-N, D-N (S: sphere; D: disc; P b/a: spheroid prolate with b/a ratio; N: needle)
dots: Monte Carlo calculation
dashed line (--): model (Eqs. 7-9)
solid line: model (Eq. 10)

Figure 4: dimensionless rate constant of collision $K_{12,N}$ as a function of $h=X_2/X_1$ ratio for various pairs of particles with different shapes: P 0.2-N and P 0.05-N.
dots: Monte Carlo calculation
solid line: model (Eqs. 10 and 16a-b)

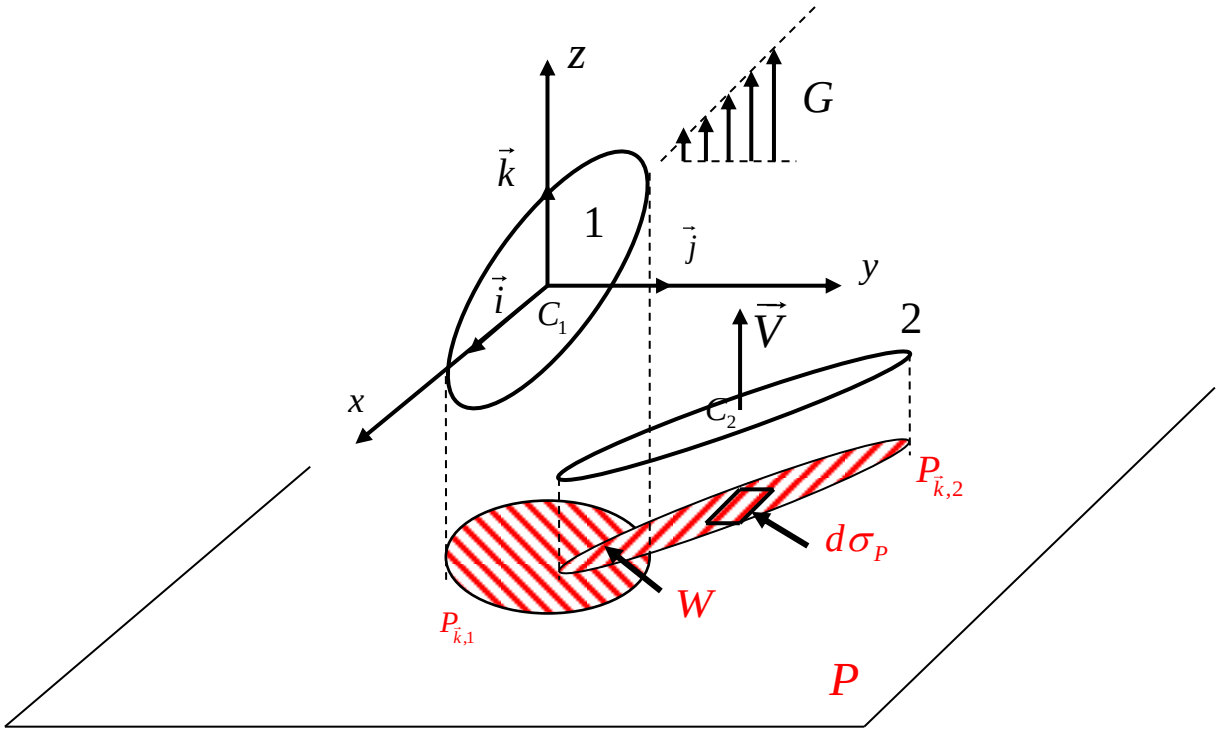

Figure 1

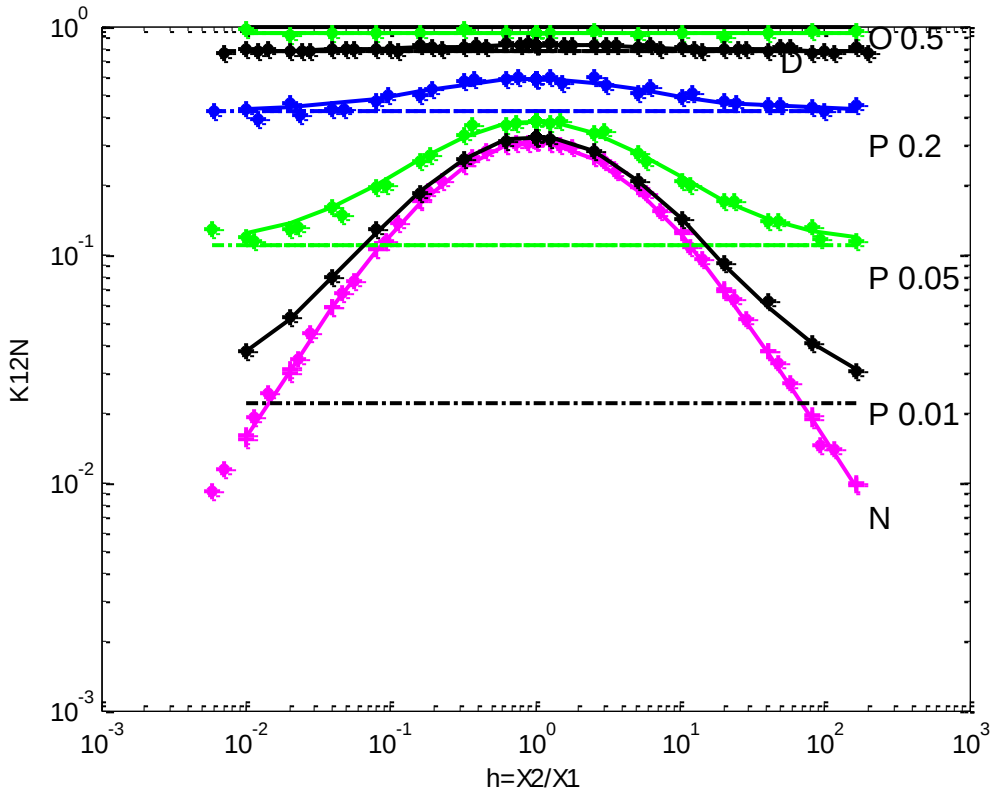

Figure 2

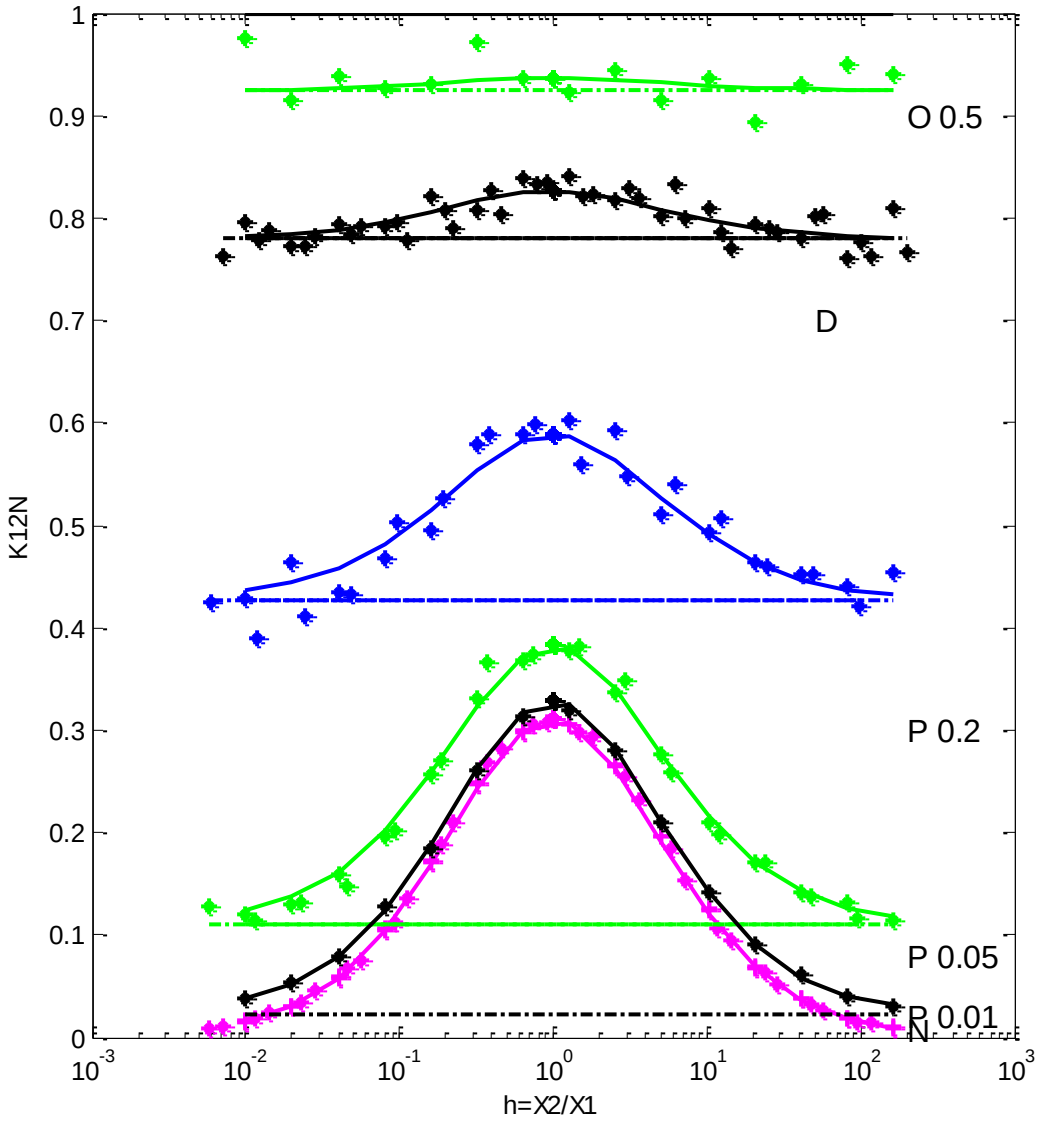

Figure 2 (zoom)

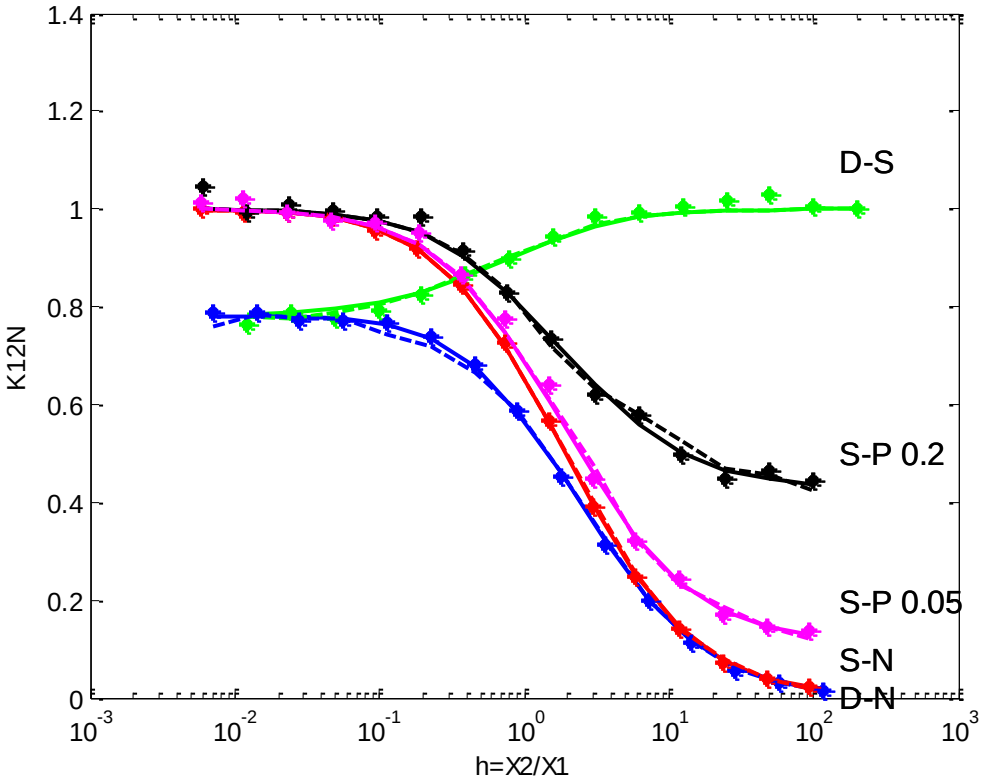
1.4
1.2
1
0.8
0.6
0.4
0.2
0
K12N
D-S
S-P 0.2
S-P 0.05
S-N
D-N
10^-3
10^-2
10^-1
10^0
10^1
10^2
10^3
h=X2/X1

Figure 3

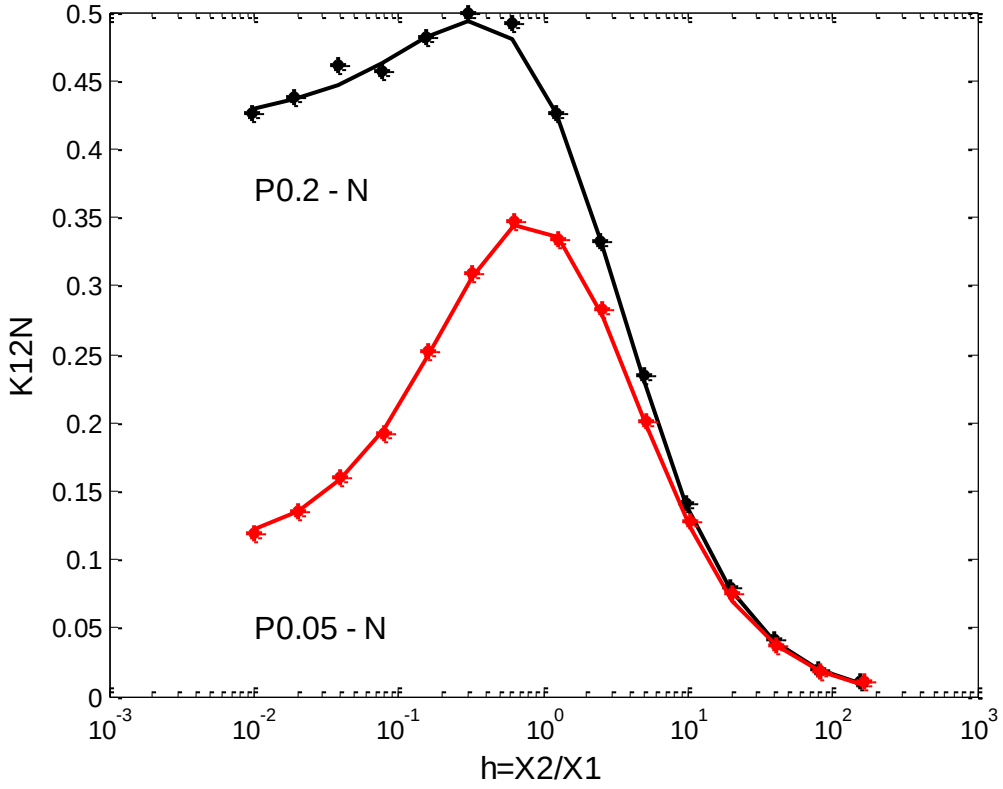
K12N
h=X2/X1
P0.2 - N
P0.05 - N
0.5
0.45
0.4
0.35
0.3
0.25
0.2
0.15
0.1
0.05
0
10^-3
10^-2
10^-1
10^0
10^1
10^2
10^3

Figure 4

Tables

Y	O 0.5	O 0.2	D	P 0.2	P 0.05	P 0.01	N
$K_{12,N}^{i-i}(0)$	0.925	0.824	0.780	0.428	0.110	0.0221	0.000
$K_{12,N}^{i-i}(1)$	0.936	0.864	0.827	0.590	0.383	0.329	0.3084

Table 1: analytical values for $K_{12,N}^{i-i}(0)$ and values coming from Monte Carlo calculations for $K_{12,N}^{i-i}(1)$ for any Y object shape

Function	1	*(k+l)/2*	*((k+l)/2)^3*	*(kl)^2*
P_j	0	2.200 (2.100/2.299)	-2.523 (-2.820/-2.226)	1.323 (1.116/1.529)
Q_j	0.3084	-0.7570	0.9371 (0.7962/1.0780)	-0.4885 (-0.5890/-0.3880)

Table 2: P_j and Q_j coefficients (Eqs.12a,b), adjusted values and (95% confidence intervals) P_1, P_2, P_3 from the multilinear regression, $P_0 = 1-(P_1+P_2+P_3)$; Q_2, Q_3 from the multilinear regression $Q_0 = 0.3084 - P_0$, $Q_1 = -(Q_0+Q_2+Q_3)$.

	Adjustment	Validation	*RMSE*	R^2
Eq. 10	D - S			
Determination of *m,n,p*	S – P0.2			
Pairs of particles	S – P0.05		0.015	0.998
	S - N			
	D - N			
Eq.16	P0.01			
Determination of *Pj* and *Qj*	P0.05			
Particles	P0.2			
	D		*Pj:* 0.0047	*Pj*: 0.9999
	O0.2		*Qj*: 0.0027	*Qj*: 0.9996
	O0.5			
	N			
Eq.10 + Eq.16		P0.05 - N	0.0086	0.994
Pairs of particles		P0.2 - N	0.0075	0.9984

Table 3: sets of data used for adjustment and validation (S: sphere; O b/a: spheroid oblate with b/a ratio; D: disc; P b/a: spheroid prolate with b/a ratio; N: needle)

Nomenclature (main notations)

a : length of the MCS box

a_i, b_i, c_i : geometrical characteristics of the particle i

a_p, b_p : geometrical characteristics of the particle projection

A_j : random number

CV : coefficient of variation

f_j : function (Eq. 13)

G : shear rate

h : ratio of two size parameters

i, j : particle indices (=1,2)

$\vec{i}, \vec{j}, \vec{k}$: axis unit vectors

K_{12} : collision rate constant

$K_{12,N}$: dimensionless collision rate constant

$K_{12,N}^{i-i}$: $K_{12,N}$ for two particles with the same shape

$K_{12,N}^{i-j}$: $K_{12,N}$ for two particles with any shapes

k, l : shape parameters $k = b/a, l = c/a$

L, L_p : needle length, length of the needle projection

n, m, p : exponents

N_r, N_c : number of MC runs, number of effective collisions

$O_i\left(\theta_i, \phi_i\right)$: orientation of the particle i

P, Q : functions (Eqs 11a,b)

P_j, Q_j : coefficients (Eqs 12a,b)

$R_{g,i}$: gyration radius of particle *i*

$R^2, Q^2, RMSE, SSE$: classical parameters of the statistical analysis

$\vec{V}$: particle velocity

x, y, z : coordinates

X_i : size parameter of particle *i* (Eq.2)

λ_i : anisotropy parameter of particle *i* (Eq.3)

σ : standard deviation